Construction and Building Materials 106 (2016) 198–208

Contents lists available at ScienceDirect

Construction and Building Materials

journal homepage: www.elsevier.com/locate/conbuildmat

# Fatigue behavior of corroded prestressed concrete beams

Weiping Zhang, Xiguang Liu, Xianglin Gu *

*Department of Structural Engineering, Tongji University, 1239 Siping Road, Shanghai 200092, PR China*

## HIGHLIGHTS

- Fatigue tests were conducted on corroded prestressed concrete beams.
- The 3D geometric models of corroded wires or rebars were obtained.
- Fatigue failure mechanism of corroded prestressed concrete beams was revealed.
- Longitudinal variation of the cross-sectional area had a significant influence on fatigue behavior of corroded beams.

## ARTICLE INFO

*Article history:*
Received 10 April 2015
Received in revised form 17 November 2015
Accepted 16 December 2015

*Keywords:*
Prestressed concrete beam
Corrosion
Fatigue
Fracture

## ABSTRACT

This paper presents the results of an experimental study on the fatigue behavior of pretensioned partially prestressed concrete beams with corroded prestressing wires or rebars. A three-dimensional laser scanning technique was employed to obtain the geometric models of corroded prestressing wires or rebars. It was observed that fatigue cracks initiated and propagated rapidly around corrosion pits under cyclic loading. The cyclic loading led to fatigue fracturing of the prestressing wires (rebars) at the minimum cross-section where the corrosion pits had formed. With the increased corrosion of the prestressing wires, the sooner fracture of the first wire and the shorter interval between the failures of the two wires in the test beam were found, resulting in a shorter fatigue life of the beam. A higher partially prestressed ratio or load range brought a larger stress level, stress range, and thus a shorter fatigue life of corroded beams. Compared with the uncorroded beam, it was also found that the corroded beams exhibited a faster stiffness degradation and development of deflections and crack widths under cyclic loading.



## 1. Introduction

Corrosion of prestressing steel is one of the primary reasons in the deterioration of prestressed concrete structures. Prestressing steel experiences a continuous applied stress level of about 55–65% of its ultimate tensile strength throughout its life [1,2], and corrosion-initiated loss in cross-sectional area often results in local yielding and fracture. Fracture of prestressing steel may lead to brittle failure of structural members and even catastrophic failure of entire bridges, as seen in the sudden collapse of the Ynys-y-Gwas Bridge [3]. Costly rehabilitation of such deteriorated structures is necessary to prevent further damage. It has been reported that one in nine bridges in the United States are rated as structurally deficient, and an annual investment of 20.5 billion US dollars is needed to repair them [4].

Much research has been focused on the static flexural behavior of prestressed concrete beams with corroded prestressing steel. Corroded prestressing steel always fails at the minimum cross-sectional area in tensile tests with significant degradation in deformability and load capacity [5–7]. Bond deterioration between corroded prestressing strands and concrete has also been found in pull-out tests [8]. Static test results have indicated a notable reduction in deformation and load capacity, as well as a premature brittle failure mode of corroded prestressed concrete beams [9–14]. Randomly distributed corrosion pits were found along the length of a steel bar, and the difference between the minimum and average cross-sectional area were observed to increase with the increase of corrosion [15]. Further observations determined that corroded prestressed concrete beams may fail at cross-sections that have not been subjected to the maximum moment, causing the failure probability in both strength and serviceability to be increased [16].

Prestressed concrete bridges are also subjected to fatigue loading during their service life, and the cyclic variation in stress of the bottom prestressing steel in bridge girders is generated by traffic

* Corresponding author.
*E-mail addresses:* weiping_zh@tongji.edu.cn (W. Zhang), xiguang830@163.com (X. Liu), gxl@tongji.edu.cn (X. Gu).

http://dx.doi.org/10.1016/j.conbuildmat.2015.12.119
0950-0618/

loading at a relatively high frequency. High-cycle tension fatigue tests of corroded rebars showed that fatigue behavior is more sensitive to corrosion than static tensile behavior, and that fatigue life decreases significantly due to corrosion [17]. Corroded bridge cables from both aged bridges and an accelerated corrosion process were tested by high-cycle fatigue loading, fatigue cracks initiated around corrosion pits due to stress concentration and fatigue life decreased notably [18,19]. Corroded reinforced concrete beams under fatigue loading exhibited a brittle failure, and their flexural stiffness and fatigue life decreased with the increase of corrosion degree [20–22]. Prestressed concrete girders are widely used in bridges with a higher stress level, but few fatigue tests have been conducted on corroded prestressed concrete beams.

This paper presents an experimental investigation on the fatigue behavior of corroded prestressed concrete beams. Thirteen pretensioned partially prestressed concrete beams corroded through the impressed current method were considered. Both static and fatigue tests were conducted with corroded and uncorroded beams. The effects of corrosion degree of prestressing wires or rebars, the partial prestressing ratio (PPR), and the load range on fatigue behavior of corroded beams were also analyzed and discussed. After failure of the corroded beams under cyclic loading, the corroded prestressing wires or rebars were taken out from the beams, and scanned by a three-dimensional laser scanner. The 3D geometric models were obtained to analyze the influence of longitudinal variation of the cross-sectional areas on fatigue behavior of corroded beams. The scanning electron microscope (SEM) was used to perform a fractography analysis of the fractured surfaces.

## 2. Experimental program

### 2.1. Specimens design and fabrication

The experimental program consisted of testing 13 pretensioned partially prestressed concrete beams. All beams were of the same size with a cross section of 150 × 300 mm and a length of 2700 mm. Beam dimensions and cross-section details are shown in Fig. 1. All beams were simply supported with a span of 2400 mm and loaded at two symmetrical third-point loads.

Three uncorroded beams were tested under static loading to obtain the ultimate load capacity, which were used to determine the minimum and maximum loads of fatigue tests. One uncorroded and nine corroded beams were tested under cyclic loading at a constant load range. The test variables included the corrosion degree of prestressing wires or nonprestressed longitudinal rebars, PPR and load range. The PPR is defined as follows:

$$\mathrm{PPR} = \frac{(M_u)_p}{(M_u)_{p+s}} \quad (1)$$

where $(M_u)_p$ is the ultimate moment contributed by the prestressing wires and $(M_u)_{p+s}$ is the ultimate moment contributed by both prestressing wires and tension rebars.

Gravimetric mass loss was used to quantify corrosion degrees for the convenience of engineering applications. Four target corrosion degrees of prestressing wires, three target corrosion degrees of nonprestressed tension rebars and three levels of PPR were considered, as shown in Table 1. The load ranges were 30%, 45% or 50% of the ultimate load capacity of the uncorroded control beams tested under static loading, where the same minimum load was equal to 10% of the ultimate load capacity. Thus, the maximum loads were 40%, 55% or 60% of the ultimate load capacity, similar to service load in engineering practices.

Two 7-mm-diameter low-relaxation prestressing wires ran straight through all the beams. The nonprestressed longitudinal rebars consisted of two hot rolled ribbed bars with a nominal diameter of 12, 14, or 16 mm, respectively. Furthermore, two hot rolled ribbed bars with a diameter of 10 mm were used as compression steel. Bottom and side cover thickness was 25 mm. A diameter of 10 mm plain stirrups spaced at 100 mm in the shear zone and 200 mm in the flexural zone were used as shear reinforcement so that the beams were expected to fail in the flexural mode. Additional chuck anchors for individual prestressing wires near the ends of the beams were placed to reduce the slip between prestressing wires and concrete. Confining reinforcements in the form of spirals were placed in the concrete directly behind the anchors, as shown in Fig. 1. Mechanical properties of prestressing wires and steel bars were tested, and the results are given in Table 2. The concrete was designed for a 28-day nominal cubic compressive strength of 40 MPa. The cement, water, aggregate and sand proportions by weight were: 1:0.36:2.87:1.48.

Beams were made in several batches using a specially designed steel formwork, which can be used to pretension prestressing wires. Each prestressing wire was pretensioned individually up to 75% of its nominal ultimate tensile strength. Strain gauges were used to monitor the variation of wire strains during the whole process of pretensioning and releasing. Approximately 24 h after pretensioning, the concrete were cast. Cubic concrete blocks in 150 × 150 × 150 mm and prism concrete blocks in 150 × 150 × 300 mm were cast using the same concrete as that in the beams. The cast beams and concrete blocks were wet-cured under the same condition. Cubic concrete blocks were used to obtain the compressive strength of the concrete at release and after 28 days for each set of beams. The compressive strength and modulus of elasticity of concrete in each individual beam at the time of testing were determined from the prism concrete blocks, as shown in Table 3. The pretensioned wires were released after the concrete strength had reached at least 85% of its designed strength from cubic blocks tests. The release of the prestressing wires was accompanied by cutting the wires with an oxygen torch. The effective stress in the prestressing wires after releasing was around 57–72% of the nominal ultimate tensile strength, as shown in Table 1.

### 2.2. Accelerated corrosion process

The accelerated corrosion process was started by immersing the beams partially into a solution of 5% sodium chloride with wires or rebars about 50 mm above the solution. To keep stirrups from corroding, an epoxy cloth covering was used at locations where the stirrups contact with the longitudinal steel bars, and nylon cable ties were used instead of steel wires during assembly of reinforcement cages. The wires or rebars were then connected to the positive terminal of a DC galvanostatic power supply, while the copper plate placed underneath the solution was connected to the negative terminal. Fig. 2 shows a built-in ammeter and potentiometer in the power supply used to monitor and control the current intensity. The applied current density was kept at approximately 100 μA/cm$^2$ [23]. In compliance with Faraday's law, different durations of impressed current were employed to achieve various degrees of corrosion of the wires or rebars in the beams.

### 2.3. Instrumentation

Strain gauges were attached separately to the prestressing wires and rebars along their length. Strain gauges were placed on the concrete spaced vertically at 50 mm near midspan, and two gauges were placed at the top and bottom surface

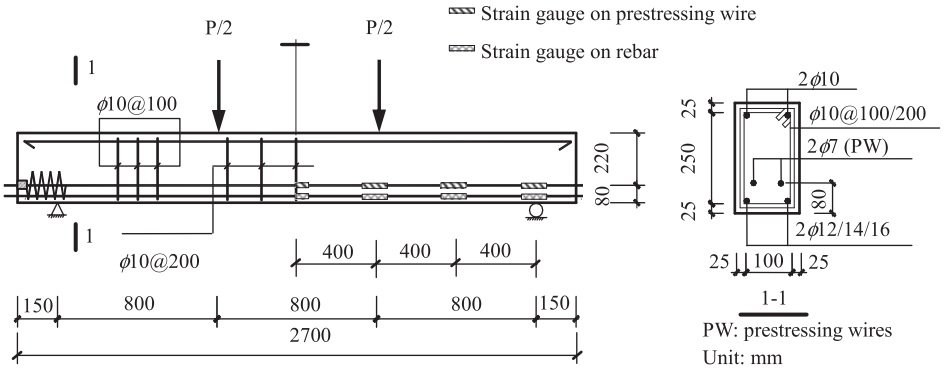


**Fig. 1.** Beam dimensions and cross-section details.

**Table 1**
Variables of the test beams.

| Beam notation | Type of load | Maximum load, $P_{min}$ (kN) | Minimum load, $P_{max}$ (kN) | Load range[a] (%) | Reinforcing steel | PPR | Target corrosion degree | | Stress levels (%) | |
|---|---|---|---|---|---|---|---|---|---|---|
| | | | | | | | PW[b] | Rebar | After tensioning | After releasing |
| PP0HS | Static | 0 | 135.0 | – | 2$\phi$12 | 0.57 | 0 | 0 | 77 | 64 |
| PP0MS | Static | 0 | 142.8 | – | 2$\phi$14 | 0.50 | 0 | 0 | 74 | 57 |
| PP0LS | Static | 0 | 168.7 | – | 2$\phi$16 | 0.43 | 0 | 0 | 75 | 64 |
| PP0MF-3 | Fatigue | 14.3 | 85.7 | 50 | 2$\phi$14 | 0.50 | 0 | 0 | 72 | 66 |
| PP1MF-3 | Fatigue | 14.3 | 85.7 | 50 | 2$\phi$14 | 0.50 | 0.025 | 0 | 75 | 58 |
| PP2MF-3 | Fatigue | 14.3 | 85.7 | 50 | 2$\phi$14 | 0.50 | 0.05 | 0 | 81 | 63 |
| PP3MF-3 | Fatigue | 14.3 | 85.7 | 50 | 2$\phi$14 | 0.50 | 0.075 | 0 | 81 | 62 |
| PP2HF-3 | Fatigue | 13.5 | 81.0 | 50 | 2$\phi$12 | 0.57 | 0.05 | 0 | 74 | 59 |
| PP2LF-3 | Fatigue | 16.9 | 101.0 | 50 | 2$\phi$16 | 0.43 | 0.05 | 0 | 74 | 59 |
| PP2MF-1 | Fatigue | 14.3 | 57.1 | 30 | 2$\phi$14 | 0.50 | 0.05 | 0 | 61 | 58 |
| PP2MF-2 | Fatigue | 14.3 | 78.5 | 45 | 2$\phi$14 | 0.50 | 0.05 | 0 | 71 | 69 |
| PS1MF-3 | Fatigue | 14.3 | 85.7 | 50 | 2$\phi$14 | 0.50 | 0 | 0.05 | 73 | 61 |
| PS2MF-3 | Fatigue | 14.3 | 85.7 | 50 | 2$\phi$14 | 0.50 | 0 | 0.10 | 78 | 72 |

[a] Load range is expressed as the percentage of the static load capacity of the uncorroded control beams.
[b] PW: prestressing wire.

**Table 2**
Mechanical properties of prestressing wires and steel bars.

| Type of reinforcement | Diameter (mm) | Yield strength (MPa) | Ultimate strength (MPa) | Elongation (%) | Modulus of elasticity (MPa) |
|---|---|---|---|---|---|
| Prestressing wires | 7 | 1650.4 | 1941.6 | 6.1 | $1.99 \times 10^5$ |
| Ordinary deformed steel bars | 10 | 470.4 | 586.2 | 27.4 | $2.01 \times 10^5$ |
| | 12 | 464.5 | 565.2 | 16.6 | $2.01 \times 10^5$ |
| | 14 | 403.8 | 542.8 | 26.5 | $2.01 \times 10^5$ |
| | 16 | 452.1 | 578.0 | 33.5 | $2.03 \times 10^5$ |
| Ordinary plain steel bars | 10 | 335.3 | 459.7 | 34.2 | $2.00 \times 10^5$ |

**Table 3**
Mechanical properties of concrete.

| Beam notation | Cubic compressive strength at release, MPa (testing age) | Cubic compressive strength at 28 days, MPa | Prism compressive strength at testing, MPa (testing age) | Modulus of elasticity at testing, GPa (testing age) |
|---|---|---|---|---|
| PP0HS | 52.9 (28 d) | 52.9 | 38.4 (45 d) | 31.4 (45 d) |
| PP0MS | 32.9 (9 d) | 44.7 | 32.4 (56 d) | 30.1 (56 d) |
| PP0LS | 52.9 (28 d) | 52.9 | 38.8 (47 d) | 31.6 (47 d) |
| PP0MF-3 | 32.9 (9 d) | 44.7 | 35.3 (80 d) | 30.7 (80 d) |
| PP1MF-3 | 32.9 (9 d) | 44.7 | 38.4 (133 d) | 31.4 (133 d) |
| PP2MF-3 | 35.3 (8 d) | 48.8 | 38.5 (127 d) | 30.3 (127 d) |
| PP3MF-3 | 35.3 (8 d) | 48.8 | 38.1 (139 d) | 30.1 (139 d) |
| PP2HF-3 | 37.0 (8 d) | 49.3 | 35.9 (117 d) | 30.6 (117 d) |
| PP2LF-3 | 32.9 (9 d) | 44.7 | 38.2 (129 d) | 31.4 (129 d) |
| PP2MF-1 | 36.8 (10 d) | 49.2 | 36.9 (84 d) | 30.8 (84 d) |
| PP2MF-2 | 36.8 (10 d) | 49.2 | 40.3 (106 d) | 32.2 (106 d) |
| PS1MF-3 | 37.0 (8 d) | 49.3 | 36.4 (123 d) | 30.5 (123 d) |
| PS2MF-3 | 37.0 (8 d) | 49.3 | 39.5 (165 d) | 31.4 (165 d) |

**Fig. 2.** Accelerated corrosion of prestressed concrete beams.

of concrete at midspan. Five displacement transducers with a 50 mm range were set at the supports, loading points and midspan to measure vertical displacements of the beams under static loading. Layout of displacement transducers and strain gauges are shown in Fig. 3.

A high-speed, high-accuracy charge coupled device (CCD) laser displacement sensor of KEYENCE® was employed to monitor the midspan deflection during the whole process of cyclic loading. Crack widths were measured by a digital crack width detector device of GTJ® with an accuracy of 0.01 mm, which includes the measurement sensor and screen.

The readings of the strain gauges and the displacement transducers were recorded using a National Instruments® PXIe-1082 data acquisition system. The data acquisition frequencies were 2 Hz and 1000 Hz for the static and fatigue loading tests, respectively.

### 2.4. Test setup and loading procedure

The fatigue tests were conducted on a servo-hydraulic Amsler® P960 pulsator testing machine comprised of a 250 kN dynamic actuator, hydraulic pump and load unit control panel. A photograph of the fatigue test setup is shown in Fig. 4. The load was measured using a 300 kN load cell.

The fatigue tests were performed under load control. Prior to conducting the cyclic loading, three static load cycles were applied. The load was gradually increased to $P_{max}$; then, it was unloaded to zero. Cracking loads, initial deflections, strains and crack widths were recorded. Then a cyclic loading with a constant load range was applied at a frequency of 4.5 Hz.

The cyclic loading was interrupted periodically at a predetermined number of cycles and then, a static cycle was applied between zero and $P_{max}$ to verify the condition of the beams. Each time the fatigue tests were interrupted for static loading, data were collected from all the instruments. Crack width was also measured during the static loading.

### 2.5. Measurement of corrosion degree

After the failure of the beams under cyclic loading, corroded wires or rebars were carefully removed from the beams. The wires or rebars were cut into pieces that ranged from 400 to 600 mm in length and then cleaned with Clark's solution, according to ASTM Standard G1-03 "Practice for preparing, cleaning, and evaluating corrosion test specimens" [24]. The cleaned steel bars were then dried in an oven for 4 h.

The degree of corrosion of the wires or rebars, $\eta_s$, was quantified based on gravimetric mass loss, i.e., the average loss of a cross-sectional area, and was calculated as the ratio of the mass loss of the steel bars due to corrosion to the original mass, as shown in Table 4. All the measured corrosion degrees were smaller than the expected values. The difference may be caused by the delayed onset of corrosion due to the concrete presence in the specimens, since the original form of Faraday's law is related to bared bars [25,26].

To achieve a deeper understanding of the influence of longitudinal distribution of the cross-sectional area along the length of wires or rebars on the fatigue behavior of the beams, a 3D laser scanning technique was employed to obtain the geometric models of the corroded wires or rebars [27–30]. Comparisons between actual morphology and the 3D geometric model of corroded wires and rebars are shown in Fig. 5. By using Pro/ENGINEER software®, the cross-sectional areas were evaluated along the length of a wire or rebar at intervals of 1 mm [15].

## 3. Fatigue failure mechanism of test beams

### 3.1. Fatigue life and failure modes

The tested ultimate load capacities of beams PP0HS, PP0MS and PP0LS were 135.0 kN, 142.8 kN and 168.7 kN, respectively. Then the minimum and maximum loads for the other ten beams in fatigue tests can be determined according to their designed load levels and ranges, as shown in Table 1.

Ten beams all failed in fatigue tests, and the failure modes are shown in Fig. 6. Nine in ten beams failed in the constant moment region at the location of the main crack except for beam PP1MF-3. Therefore, the first ruptured prestressing wires in the constant moment region of ten beams were scanned by a 3D laser scanner of Faro® to relate longitudinal distribution of corrosion pits to failure location. For beam PP1MF-3, the wire in the shear span region was also scanned.

Fatigue test results are shown in Table 4. The stress ranges reported herein were determined by multiplying the measured strains from the attached gauges by the elasticity modulus of steel bars in Table 2. The measured stress ranges of steel bars at midspan

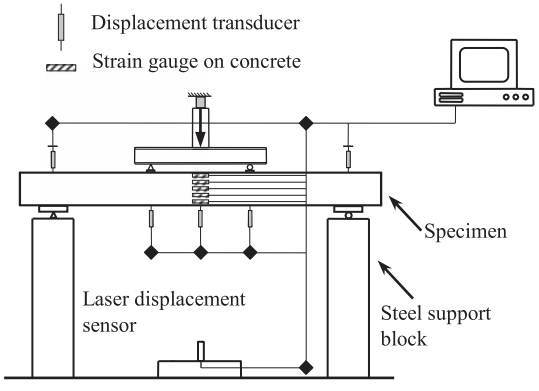


**Fig. 3.** Layout of displacement transducers and strain gauges.

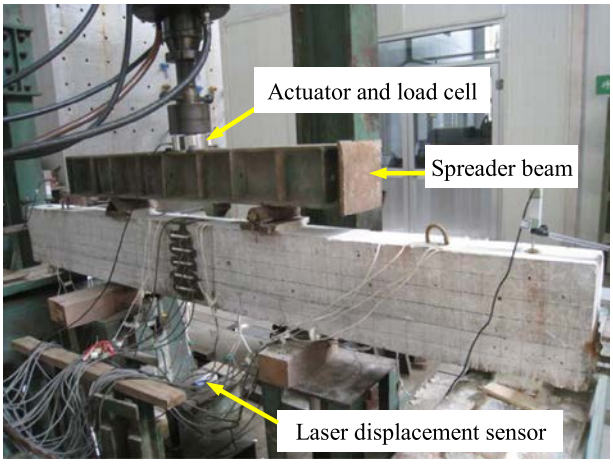


**Fig. 4.** Fatigue test setup.

may underestimate the maximum stress range experienced at the location of main cracks because the strain gauges could not coincide exactly with the main cracks. Nonetheless, an inversely proportional relationship between the measured rebar stress range and fatigue life is evident.

### 3.2. Fatigue failure of beams with uncorroded and corroded rebars

The initial stress range in longitudinal rebars is larger than that of prestressing wires because the rebar is located far away from the neutral axis. Thus, fatigue failure of uncorroded beams resulted from the fatigue fracturing of rebars.

Take the beam PP0MF-3 as an example, the initial stress range of rebars was 12% higher than prestressing wires. The fracturing of rebar occurred at approximately 1,969,000 cycles, and the beam collapsed immediately in a brittle mode. This is in agreement with previous test results [31]. The two rebars both failed at the main crack, and the fracture surface was even without obvious plastic deformation, as shown in Fig. 7. This is a common characteristic of fatigue fracture. It can be seen from a scanning electron microscope (SEM) image of the fatigue fracture surface in Fig. 8a that the fatigue crack starting from the root of one transverse rib.

For beams with corroded rebars, local stress concentration and cross-sectional area loss induced by corrosion made the rebars into a more adverse status. The longitudinal distribution of the cross-sectional area of the first ruptured rebars in the corroded beams is presented in Fig. 9, and it can be seen that the fracture of the first rebars occurred at the minimum cross-sections. The initial stress range of the rebar in beam PS2MF-3 was 123% higher than that in prestressing wires due to the reduced cross-sectional area, as shown in Table 4. Moreover, fatigue cracks initiated around corrosion pits, as shown in Fig. 8b and c. Finally, the fracture of the tension rebar occurred at the main crack after approximately 57,000 loading cycles, followed by the instant rupture of prestressing wires at the same cross-section.

### 3.3. Fatigue failure of beams with corroded prestressing wires

For beams with corroded prestressing wires, fatigue cracks also initiated and propagated rapidly around corrosion pits under cyclic loading, as shown in Fig. 10. The fracturing of corroded prestressing wires took place prior to that of uncorroded tension rebars under the same fatigue loading, even though the nominal stress range was lower in the wires. The subsequent fatigue fracturing of the residual prestressing wires and rebars took place in succession until finally, the brittle failure of the beams occurred.

**Table 4**
Fatigue test results.

| Beam notation | Initial cyclic loading | | 1st prestressing wire fracture | | | 2nd prestressing wire fracture | | Rebar fracture | Measured corrosion degree, $\eta_s$ | |
|---|---|---|---|---|---|---|---|---|---|---|
| | $\Delta\sigma_s$ (MPa) | $\Delta\sigma_p$ (MPa) | Cycles ($\times 10^4$) | $\Delta\sigma_s$ (MPa) | $\Delta\sigma_p$ (MPa) | Cycles ($\times 10^4$) | $\Delta\sigma_s$ (MPa) | Fatigue life ($\times 10^4$) | PW[a] | Rebar |
| PP0MF-3 | 164 | 146 | – | – | – | – | – | 196.9 | 0 | 0 |
| PP1MF-3 | 165 | 148 | 42.1 | 196 | – | 103.2 | 106 | 109.4 | 0.013 | 0 |
| PP2MF-3 | 169 | 103 | 21.9 | 201 | 110 | 34.3 | 230 | 39.3 | 0.025 | 0 |
| PP3MF-3 | 187 | 142 | 16.6 | 213 | 155 | 18.5 | 222 | 21.7 | 0.056 | 0 |
| PP2HF-3 | 232 | 121 | 8.6 | 257 | – | 21.8 | 286 | 25.9 | 0.040 | 0 |
| PP2LF-3 | 185 | 142 | 29.2 | 202 | – | 70.5 | 236 | 82.8 | 0.037 | 0 |
| PP2MF-1 | 106 | 58 | 188.5 | 142 | 72 | – | – | 231 | 0.013 | 0 |
| PP2MF-2 | 167 | 132 | 6.8 | 171 | 146 | 34.4 | 203 | 46.6 | 0.016 | 0 |
| PS1MF-3 | 166 | 143 | – | – | – | – | – | 25.2 | 0 | 0.034 |
| PS2MF-3 | 230 | 103 | – | – | – | – | – | 5.7 | 0 | 0.066 |

[a] PW: prestressing wire.

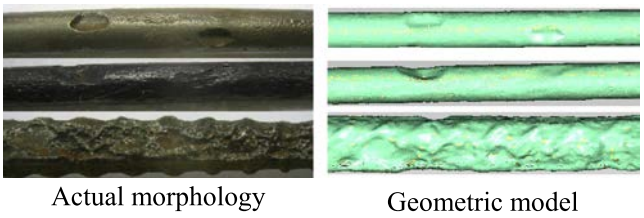


**Fig. 5.** Actual morphology and 3D geometric model of corroded wires and rebars.

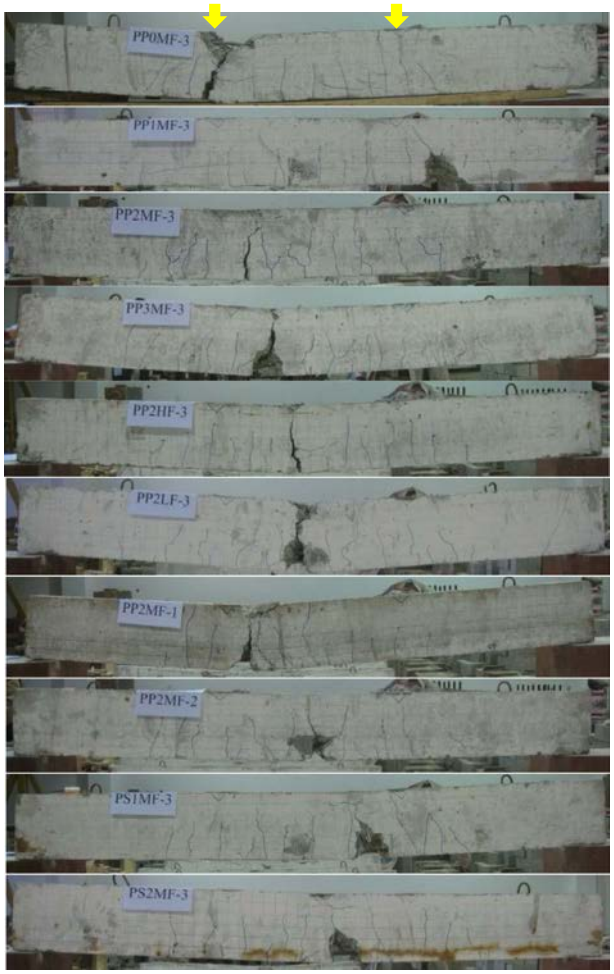


**Fig. 6.** Failure modes of beams in fatigue tests.

Figs. 11–13 present the distribution of the cross-sectional area of the first ruptured prestressing wires in the corroded beams. The fracture of the first prestressing wire occurred at the minimum cross-section where corrosion pits had formed; additionally, a sharp groove appeared in the cross-sectional area distribution curves around the failed cross-section. These curves were much steeper than those found in the other cross-sections, which resulted in high stress concentrations. Fig. 11 shows that the minimum cross-section of the first ruptured wire in beam PP1MF-3 was located in the shear span. This can reasonably explain how this beam failed at a cross-section which was not subjected to the maximum moment.

Fig. 14 is a SEM image of fatigue fracture surface of the first ruptured wire in beam PP2MF-1. The crack origin zone around the corrosion pit contained a large number of interconnected cracks and voids, which is thought to have served as a fatigue crack trigger. The propagation zone shows an apparently flat surface and contains a few fine, randomly dispersed, and isolated microscopic cracks, which were formed with the increase in loading cycles. The fatigue fracture surfaces of two wires in beam PP2MF-3 are given in Fig. 10b and d. Compared to the first fractured wire in Fig. 10b, the second fractured wire has an obviously reduced crack propagation zone as shown in Fig. 10d caused by a significant increase in stress range, which occurred after the first wire failed.

The failure process of a typical beam PP2MF-3 is described as an example in the following. Deflections and strains versus number of cycles of beam PP2MF-3 are shown in Fig. 15a and b. In the first hundred cycles there was a sharp increase in the strains of concrete and rebar. In Fig. 16, the neutral axis shifts slightly upwards, resulting in an increased midspan deflection. Then, flexural cracks alternated opening and closing stably. At the same time, midspan deflection and strain gradually increased under cyclic loading. The stable state extended to a critical point where the fracture of the first prestressing wire occurred.

The first fracturing of one wire occurred at approximately 219,000 cycles accompanied by a loud noise. Stress redistribution resulting from the fracturing of the wire was accompanied by a 33%, 16% and 6% increase in the observed maximum strain in the other wire, tension rebars and top concrete, respectively. The neutral axis shifted significantly upward and the curvature experienced a notable increase as shown in Fig. 16, leading to a 10% increase in the maximum midspan deflection. The stress ranges of tension rebars and the other wire were increased by 19% and 8%, respectively. Then, as the beam came to a relatively stable stage, deflection and strains tended to increase at a faster rate. When a subsequent fracturing of the second wire occurred at approximately 343,000 cycles, a dramatic leap in the midspan deflection and strains was observed, and then the beam came to


**Fig. 7.** Details of failed cross-sections in fatigue tests.

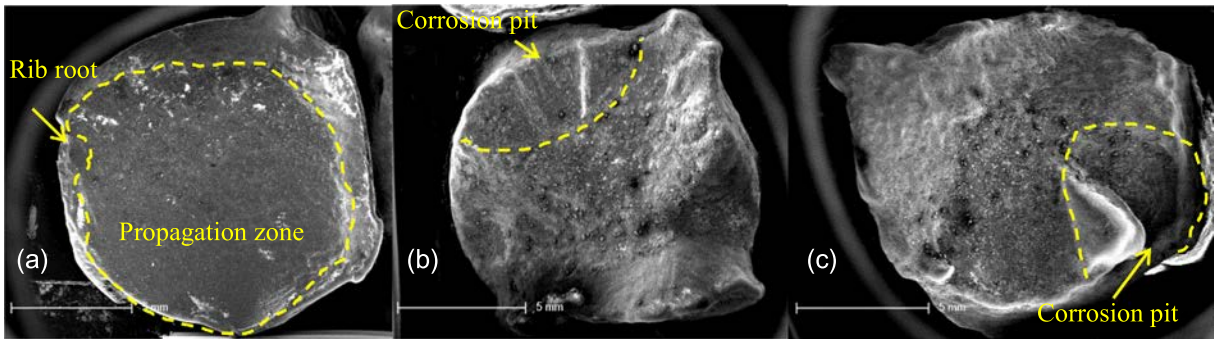


**Fig. 8.** SEM images of the fatigue fracture surfaces of rebar (a) beam PP0MF-3; (b) beam PS1MF-3; (c) beam PS2MF-3.

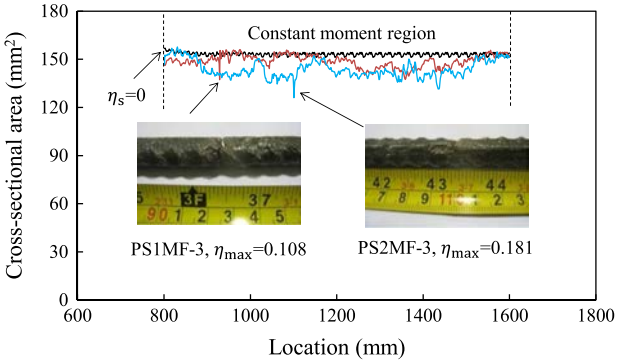


**Fig. 9.** Distribution of cross-sectional area of rebars with various corrosion degrees.

an unstable stage. Beam failure occurred after fatigue fracturing of tension rebar at approximately 393,000 cycles.

Fig. 15c shows the load–deflection curves of beam PP2MF-3 after a predetermined number of cycles during fatigue loading. It can be observed that the progressive stiffness degradation and the residual deflection increased with the increasing number of loading cycles. Crack width gradually increased at the beginning of loading, and then increased significantly after the first wire failure, as shown in Fig. 15d.

## 4. Comparative analysis of the fatigue test results

### 4.1. Influence of nonprestressed rebar corrosion

The measured average corrosion degrees of beam PS1MF-3 and beam PS2MF-3 were 0.034 and 0.066, respectively. Compared with the uncorroded beam PP0MF-3, their measured initial stress ranges of the rebars at midspan were increased by 1% and 40%, as shown in Table 4. The actual cross-sectional loss ratios at the failed cross-section beam PS1MF-3 and beam PS2MF-3 reached 0.108 and 0.181 as shown in Fig. 9, and the calculated initial stress ranges at the minimum cross-section of rebars in the constant moment region were 1.08 and 1.46 times greater than that in the uncorroded beam under the same fatigue loading. The area of the crack propagation zone of an uncorroded rebar takes up almost 75% of the cross-sectional area, as shown in Fig. 8a. Correspondingly, the propagation zone significantly decreased as the degree of corrosion increased, as shown in Fig. 8b and c. Finally, a reduction of 87% and 97% in fatigue life of beams PS1MF-3 and PS2MF-3 were caused by both cross-section loss and stress concentration, as shown in Table 4.

Deformation behavior of corroded beams with various degrees of corrosion in rebars is presented in Fig. 17. For brevity, only the development trend of deflection, strains and crack width of beams at $P_{max}$ are shown. It can be seen that corroded beams had larger deflections, strains and crack widths, which increased much faster under cyclic loading than the uncorroded beam.

### 4.2. Influence of prestressing steel corrosion

The measured average corrosion degrees of prestressing wires in beams PP1MF-3, PP2MF-3 and PP3MF-3 were 0.013, 0.025 and 0.056, respectively. It can be seen from Fig. 11 that, the actual cross-sectional loss ratios at the failed cross-section of the first wire in beams PP1MF-3, PP2MF-3 and PP3MF-3 were up to 0.087, 0.114 and 0.213, respectively. The calculated initial stress ranges at the minimum cross-section of wires in the constant moment region were 1.08, 1.13 and 1.27 times greater than that in the uncorroded beam under the same fatigue loading. Similarly, due to effects of cross-sectional loss and stress concentrations, the more severe the corrosion is, the sooner the fracture of the first wire occurs, and the shorter the interval is between two wires' failure and the lower the fatigue life of the beam. The fracturing of the first wire in three corroded beams occurred at approximately 421,000, 219,000 and 166,000 cycles, respectively. Compared with the uncorroded beam, the fatigue life of the three corroded beams had a reduction of 44%, 80% and 83% respectively, as shown in Table 4.

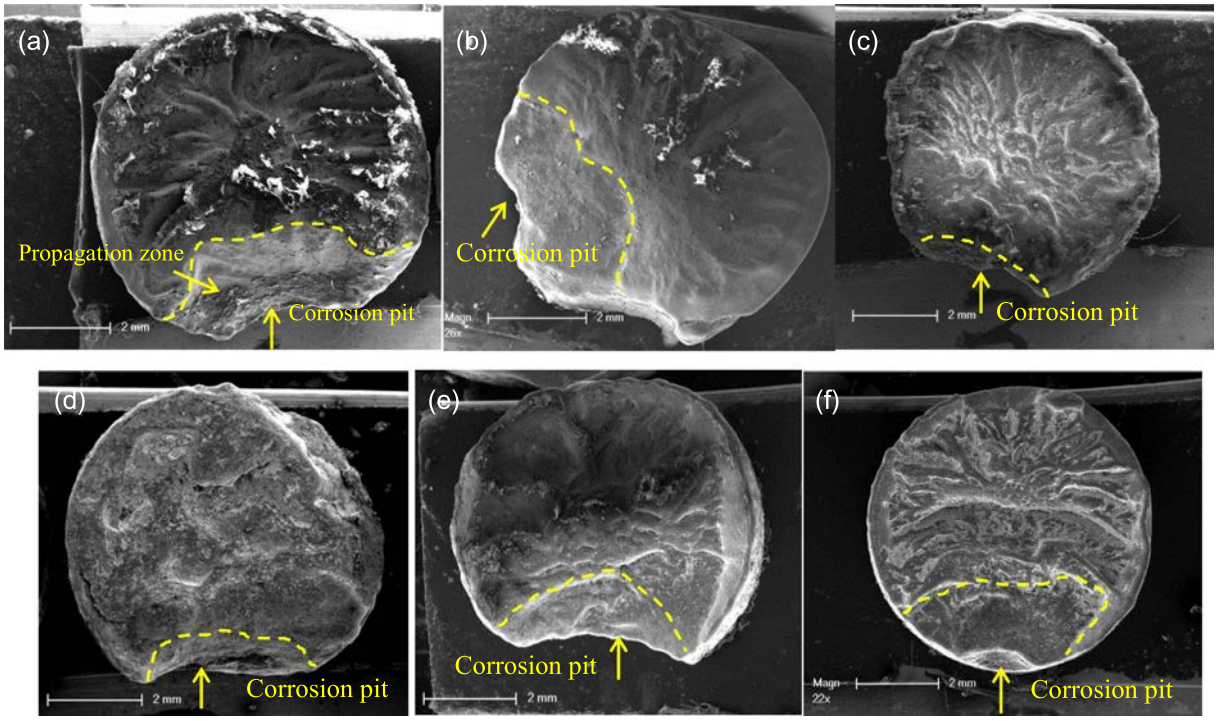


**Fig. 10.** SEM images of the fatigue fracture surfaces of wire (a) beam PP1MF-3; (b) beam PP2MF-3; (c) PP3MF-3; (d) beam PP2MF-3; (e) beam PP2HF-3; (f) beam PP2MF-1.

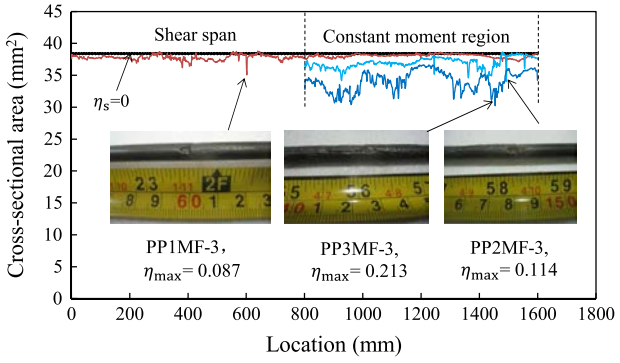


**Fig. 11.** Distribution of cross-sectional area of prestressing wires with various corrosion degrees.

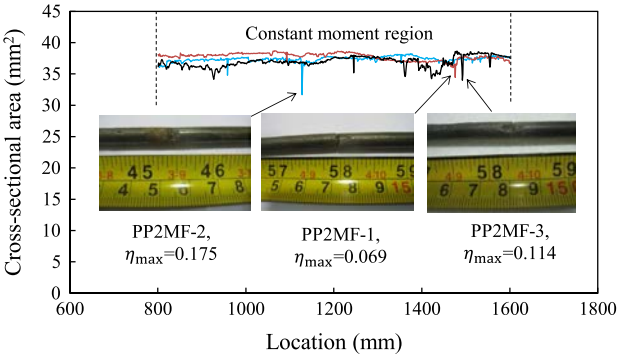


**Fig. 13.** Distribution of cross-sectional area of corroded prestressing wires for beams under different load ranges.

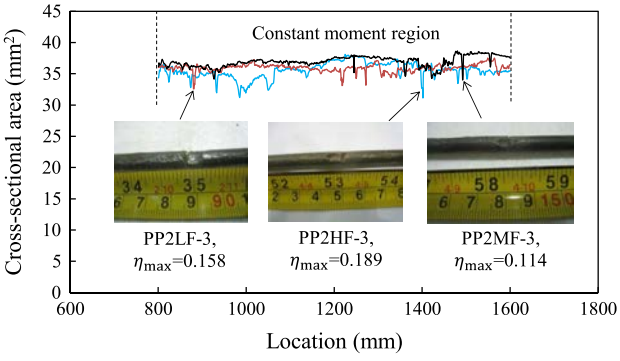


**Fig. 12.** Distribution of cross-sectional area of corroded prestressing wires for beams with different PPRs.

Deformation behavior of beams with various degrees of corroded prestressing wires at $P_{max}$ is presented in Fig. 18. Fig. 18a shows that the deflection of beams increased consistently with an increasing number of cycles, and a sudden jump and a faster increase was observed following the fracture of prestressing wires. The rebar strain, concrete strain and crack width of corroded beams shared similar development trends. Owing to the severest corrosion, the deflection and strains of beam PP3MF-3 increased faster than that occurring in the other beams.

Different from other beams, the strains of rebar and concrete in beam PP1MF-3 decreased after the second fracturing incident occurred. This is because one rebar failed in the second time, and the beam could not sustain the original fatigue load level; hence, the maximum load decreased.

Fig. 19 presents the strain distribution of the midspan section in the first cycle of cyclic loading for four beams and shows that, for the two minor corroded beams PP1MF-3 and PP2MF-3, there is little change on the top concrete fiber strain, whereas an increase in the rebar strain and crack width is evident. Therefore, the neutral axis shifts upward, and the curvature and deflection increase slightly. With a further increase in corrosion, there is an obvious increase in both the top concrete fiber strain and rebar strain of beam PP3MF-3, leading to a faster growing crack width and deflection with the increasing number of cycles.

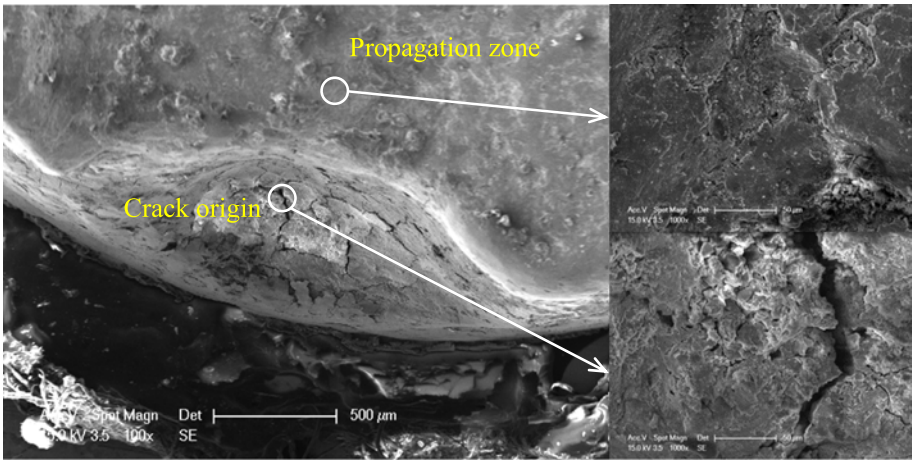


**Fig. 14.** SEM high magnification image of the fatigue fracture surface in beam PP2MF-1.

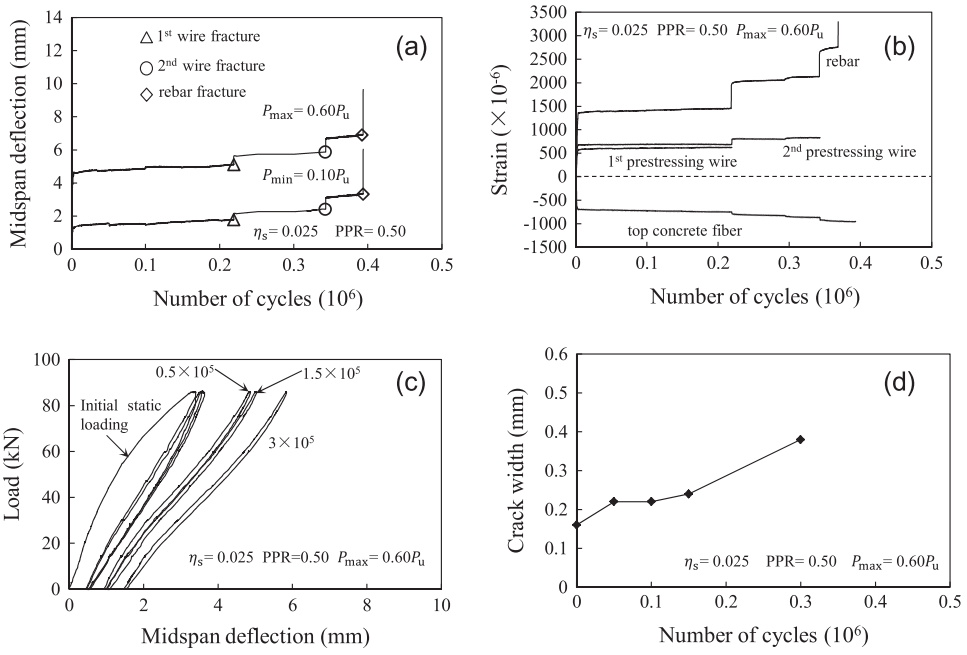


**Fig. 15.** Deformation behavior of beam PP2MF-3 (a) midspan deflection versus number of cycles; (b) strains versus number of cycles; (c) load–deflection curves at predetermined number of cycles; (d) crack width versus number of cycles.

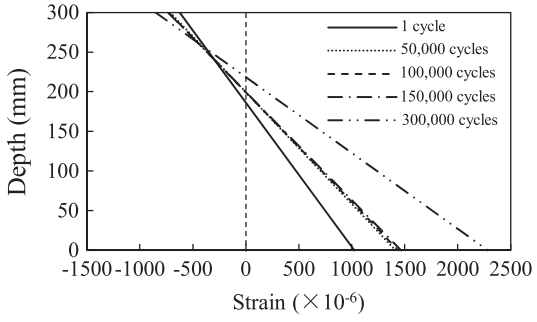


**Fig. 16.** Variations of strain distribution at midspan of beam PP2MF-3 during cyclic loading.

### 4.3. Influence of PPR

The PPR of beams PP2HF-3, PP2MF-3, and PP2LF-3 were 0.57, 0.50 and 0.43, respectively. The target corrosion degrees of prestressing wires in the three beams were all 0.05, but the measured average values were 0.040, 0.025 and 0.038, respectively.

Deformation behavior of corroded beams with different PPRs at $P_{max}$ is presented in Fig. 20. Under the same fatigue loading, beams with higher levels of PPR have a smaller area of nonprestressed steel, and therefore, a higher stress range and stress level, as presented in Table 4 and Fig. 20b. This results in an earlier fracturing of the first wire and a shorter fatigue life. Compared with beam PP2MF-3, the first fractured wire had an actual cross-sectional loss ratio of 0.189 in beam PP2HF-3, which occurred after approximately 86,000 loading cycles. Eventually, its fatigue life had a reduction of 44%, as shown in Fig. 12 and Table 4. This can be further demonstrated by the smaller propagation zone on the fatigue fracture surface, as shown in Fig. 10b and e.

For the same reason, the beam with a higher PPR exhibited a more obvious stiffness degradation and development of the deflection and crack width.

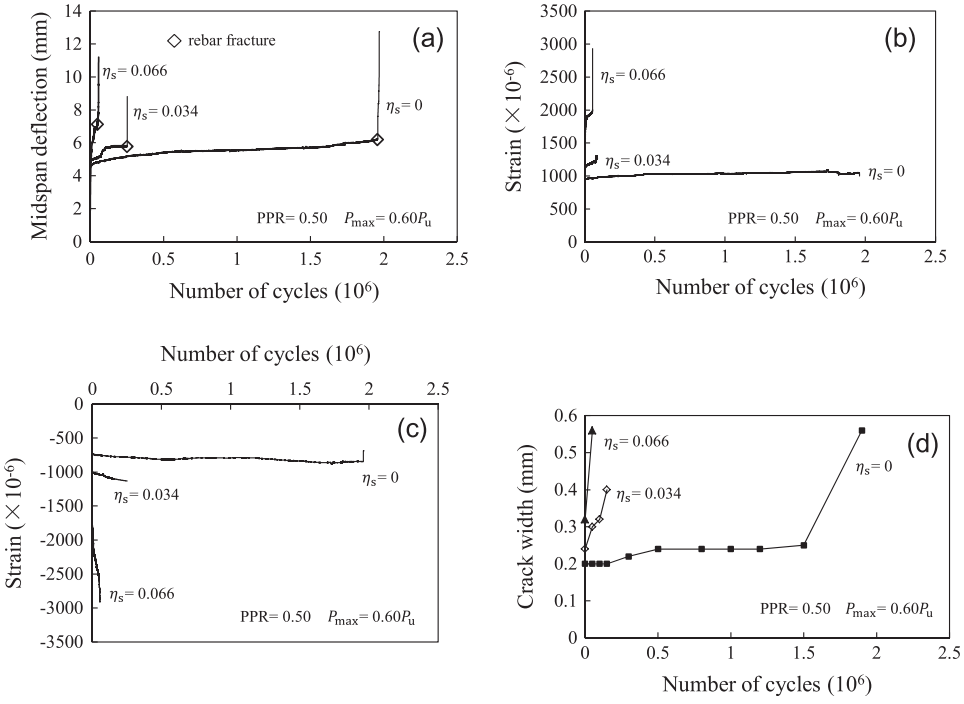


**Fig. 17.** Deformation behavior of beams with various degrees of corroded rebars at $P_{max}$ (a) midspan deflection versus number of cycles; (b) rebar strain versus number of cycles; (c) top concrete fiber strain versus number of cycles; (d) crack width versus number of cycles.

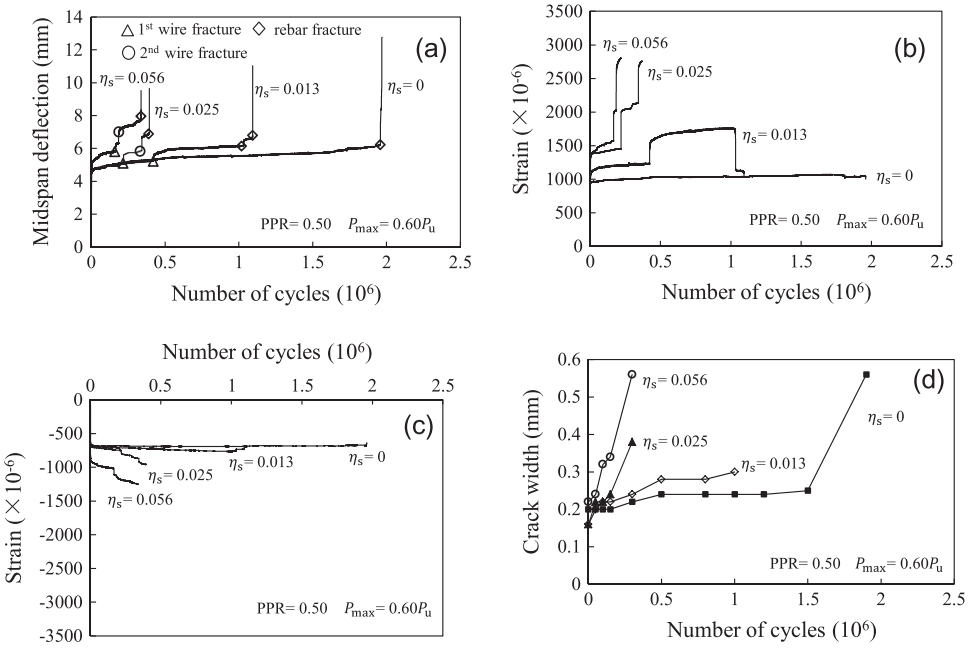


**Fig. 18.** Deformation behavior of beams with various degrees of corroded prestressing wires at $P_{max}$ (a) midspan deflection versus number of cycles; (b) rebar strain versus number of cycles; (c) top concrete fiber strain versus number of cycles; (d) crack width versus number of cycles.

### 4.4. Influence of load range

The target corrosion degrees of prestressing wires in beams PP2MF-1, PP2MF-2 and PP2MF-3 were the same, i.e., 0.05, and the measured average values were 0.013, 0.016 and 0.025, respectively. The maximum loads of the three corroded beams were 40%, 55% or 60% of the ultimate load capacity, respectively.

It can be observed from Table 4 and Fig. 21 that an increase in the maximum load caused an increase in the stress range and stress levels of prestressing wires, leading to a fast growth of fatigue cracks and an increase in granular rough zones before final fatigue fracture, as shown in Fig. 10b and f. Correspondingly, a

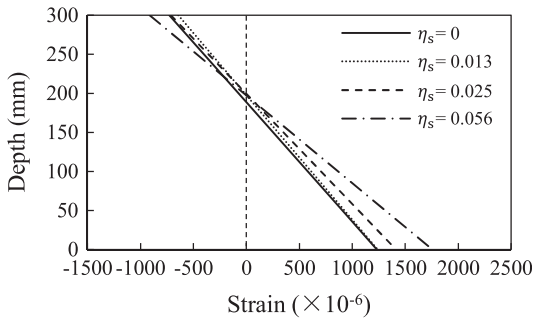


**Fig. 19.** Strain distribution at midspan in the first cycle loading.

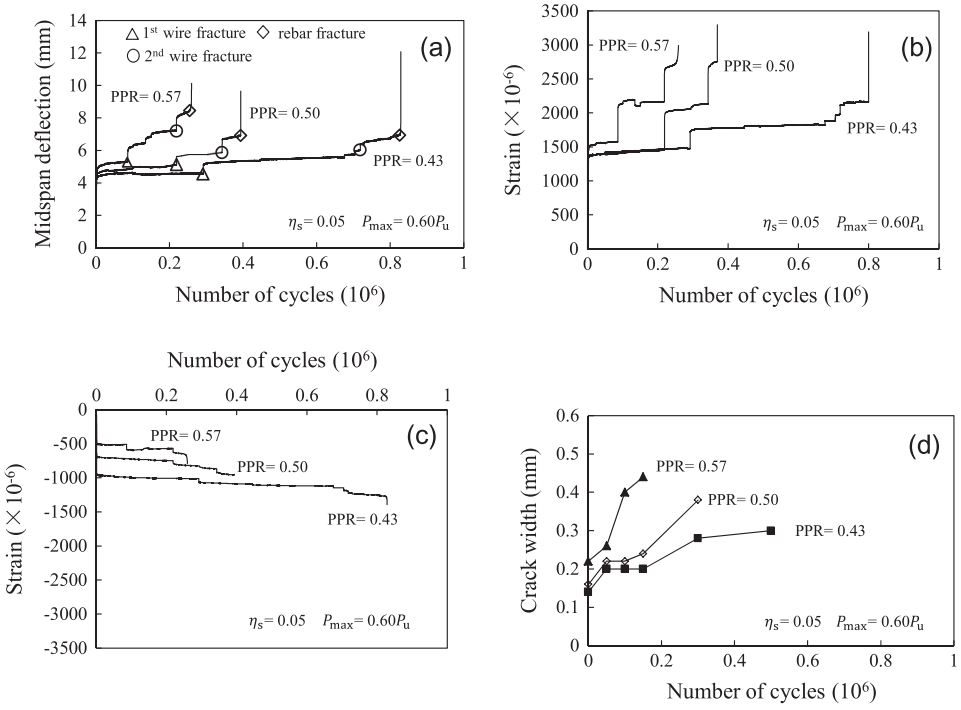


**Fig. 20.** Deformation behavior of corroded beams with different PPRs at $P_{max}$ (a) midspan deflection versus number of cycles; (b) rebar strain versus number of cycles; (c) top concrete fiber strain versus number of cycles; (d) crack width versus number of cycles.

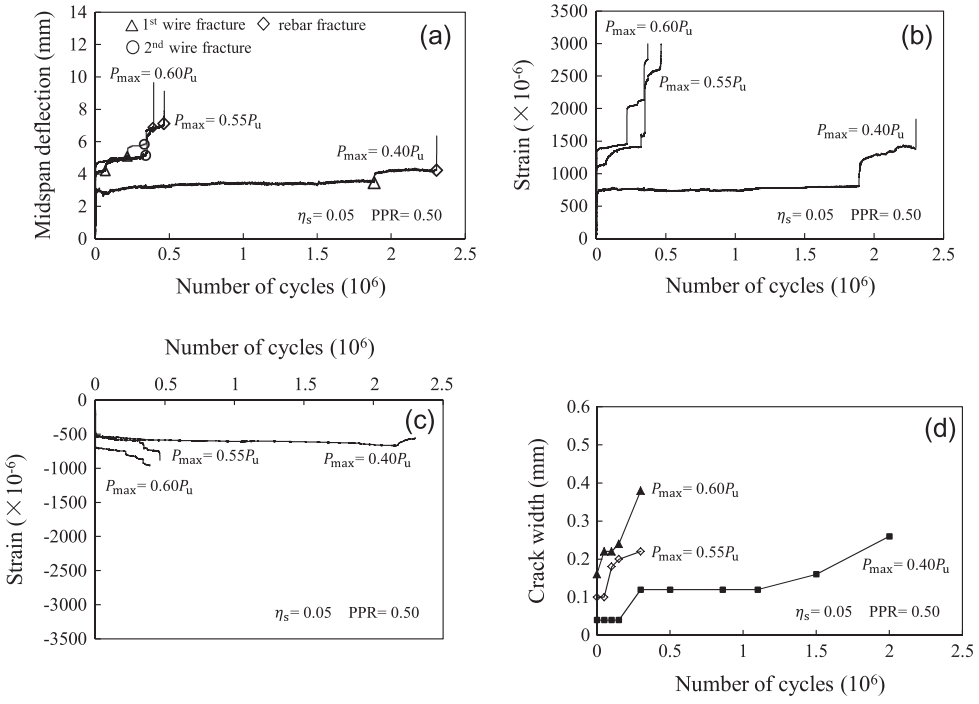


**Fig. 21.** Deformation behavior of corroded beams at $P_{max}$ under different load ranges (a) midspan deflection versus number of cycles; (b) rebar strain versus number of cycles; (c) top concrete fiber strain versus number of cycles; (d) crack width versus number of cycles.

decrease in fatigue life was observed. Similarly, as the maximum load increased, the beam exhibited a faster stiffness degradation and development of deflection and crack width under cyclic loading.

Fig. 13 shows that the fractured cross-sectional area of the first wire in beam PP2MF-2 ($\eta_{max}$ = 0.175) was much smaller than that in beam PP2MF-3 ($\eta_{max}$ = 0.114) due to uneven corrosion, which resulted in a larger stress range and an earlier fracture—even with a smaller load range.

## 5. Conclusions

Longitudinal variation of the cross-sectional area had a significant influence on the fatigue behavior of corroded beams. The

maximum cross-sectional loss ratio can be up to 10 times greater than the average degree of corrosion. All corroded beams failed at the minimum cross-section of one of the corroded rebars or wires, which might not be subjected to the maximum action.

Fatigue cracks of corroded rebars initiated and propagated rapidly around corrosion pits under cyclic loading, instead of at the root of transverse ribs for uncorroded ones. For the beams subjected to the same fatigue loading, the crack propagation zone of corroded rebars significantly decreased with the increasing degree of corrosion, leading to a shorter fatigue life.

For beams with corroded prestressing wires, their failure started from the fatigue fracture of prestressing wires instead of longitudinal rebars for corresponding uncorroded beams. The more severe the corrosion in prestressing wires is, the sooner the fracture of the first wire occurs, and the shorter the interval is between two wires' failure and the lower the fatigue life of the beam were observed. With the increased corrosion of the prestressing wires, the deflection, strain and crack width exhibited a faster increase.

With a larger PPR or load range, the rebars or prestressing wires in corroded beams had a larger range and higher stress levels, which always led to a faster stiffness degradation and a shorter fatigue life.

## Acknowledgements

This research project was financially supported by the National Basic Research Program of China (973 Program) (Grant No. 2015CB057703) and the National Natural Science Foundation of China (Grant No. 51320105013).

## References

[1] CEB-FIP, Durability of post-tensioning tendons. Lausanne: fib, 2005.
[2] ACI Committee 222, Corrosion of prestressing steels. Farmington Hills, American Concrete Institute, 2010.
[3] R.J. Woodward, D.L.S. Wilson, Deformation of segmental post-tensioned precast bridges as a result of corrosion of the tendons, Proc. Inst. Civ. Eng. 90 (1991) 397–419.
[4] American Society of Civil Engineers (ASCE), Report Card for America's Infrastructure, 2013.
[5] M.S. Darmawan, M.G. Stewart, Effect of pitting corrosion on capacity of prestressing wires, Mag. Concr. Res. 59 (2) (2010) 131–139.
[6] Y.H. Zeng, X.L. Gu, W.P. Zhang, Q.H. Huang, Study on mechanical properties of corroded prestressed tendons, J. Build. Mater. 13 (2) (2010) 169–174. 209. (in Chinese).
[7] M.M. Kashani, L.N. Lowes, A.J. Crewe, N.A. Alexander, Finite element investigation of the influence of corrosion pattern on inelastic buckling and cyclic response of corroded reinforcing bars, Eng. Struct. 75 (2014) 113–125.
[8] F. Li, Y. Yuan, Effects of corrosion on bond behavior between steel strand and concrete, Constr. Build. Mater. 38 (2013) 413–422.
[9] D. Coronelli, A. Castel, N.A. Vu, R. François, Corroded post-tensioned beams with bonded tendons and wire failure, Eng. Struct. 31 (8) (2009) 1687–1697.
[10] Z. Rinaldi, S. Imperatore, C. Valente, Experimental evaluation of the flexural behavior of corroded P/C beams, Constr. Build. Mater. 24 (11) (2010) 2267–2278.
[11] A. Castel, R. François, D. Coronelli, Response of corroded prestressed beams with bonded strands, Proc. ICE-Struct. Build. 165 (5) (2012) 233–244.
[12] R.A. Rogers, L. Wotherspoon, S. Allan, J.M. Ingham, Residual strength assessment and destructive testing of decommissioned concrete bridge beams with corroded pretensioned reinforcement, PCI J. 100–118 (2012).
[13] R.E. Melchers, T.M. Pape, Performance of 45-year-old corroded prestressed concrete beams, Proc. ICE-Struct. Build. 166 (10) (2013) 547–559.
[14] L. Wang, X. Zhang, J. Zhang, Y. Ma, Y. Xiang, Y. Liu, Effect of insufficient grouting and strand corrosion on flexural behavior of PC beams, Constr. Build. Mater. 53 (2014) 213–224.
[15] W.P. Zhang, B.B. Zhou, X.L. Gu, H.C. Dai, Probability distribution model for cross-sectional area of corroded reinforcing steel bars, J. Mater. Civ. Eng. 26 (5) (2014) 822–832.
[16] M.S. Darmawan, M.G. Stewart, Spatial time-dependent reliability analysis of corroding pretensioned prestressed concrete bridge girders, Struct. Saf. 29 (1) (2007) 16–31.
[17] W.P. Zhang, X.B. Song, X.L. Gu, S.B. Li, Tensile and fatigue behavior of corroded rebars, Constr. Build. Mater. 34 (2012) 409–417.
[18] H. Li, C.M. Lan, Y. Ju, D.S. Li, Experimental and numerical study of the fatigue properties of corroded parallel wire cables, J. Bridge Eng. 17 (2) (2011) 211–220.
[19] S. Nakamura, K. Suzumura, Experimental study on fatigue strength of corroded bridge wires, J. Bridge Eng. 18 (3) (2013) 200–209.
[20] W. Yi, S.K. Kunnath, X. Sun, C. Shi, F. Tang, Fatigue behavior of reinforced concrete beams with corroded steel reinforcement, ACI Struct. J. 107 (5) (2010) 526.
[21] Y. Ma, Y. Xiang, L. Wang, J. Zhang, Y. Liu, Fatigue life prediction for aging RC beams considering corrosive environments, Eng. Struct. 79 (2014) 211–221.
[22] J. Sun, Q. Huang, Y. Ren, Performance deterioration of corroded RC beams and reinforcing bars under repeated loading, Constr. Build. Mater. 96 (2015) 404–415.
[23] T.A. El Maaddawy, K.A. Soudki, Effectiveness of impressed current technique to simulate corrosion of steel reinforcement in concrete, J. Mater. Civ. Eng. 15 (1) (2003) 41–47.
[24] ASTM G1-03, Standard Practice for Preparing, Cleaning, and Evaluating Corrosion Test Specimens, ASTM, 2011.
[25] S. Imperatore, Z. Rinaldi, Mechanical behavior of corroded rebars and influence on the structural response of R/C elements, in: Proc. of the 2nd Int. Conf. on Concrete Repair, Rehabilitation and Retrofitting, Cape Town, South Africa, 24–26 November, CRC Press, Balkema, 2008.
[26] A. Meda, S. Mostosi, Z. Rinaldi, P. Riva, Experimental evaluation of the corrosion influence on the cyclic behaviour of RC columns, Eng. Struct. 76 (2014) 112–123.
[27] M.M. Kashani, A.J. Crewe, N.A. Alexander, Use of a 3D optical measurement technique for stochastic corrosion pattern analysis of reinforcing bars subjected to accelerated corrosion, Corros. Sci. 73 (2013) 208–221.
[28] M.M. Kashani, A.J. Crewe, N.A. Alexander, Nonlinear cyclic response of corrosion-damaged reinforcing bars with the effect of buckling, Constr. Build. Mater. 41 (2013) 388–400.
[29] M.M. Kashani, P. Alagheband, R. Khan, S. Davis, Impact of corrosion on low-cycle fatigue degradation of reinforcing bars with the effect of inelastic buckling, Int. J. Fatigue 77 (2015) 174–185.
[30] M.M. Kashani, A.K. Barmi, V.S. Malinova, Influence of inelastic buckling on low-cycle fatigue degradation of reinforcing bars, Constr. Build. Mater. 94 (2015) 644–655.
[31] M.E. Shahawi, B.D. Batchelor, Fatigue of partially prestressed concrete, J. Struct. Eng. 112 (3) (1986) 524–537.